ARCHITECTURE CIVIL ENGINEERING ENVIRONMENT
The Silesian University of Technology
No. 4/2023

doi: 10.2478/ACEE-2023-0055

ANALYSIS OF APPLICATION OF GRADIENT CONCRETE MODELS TO ASSESS CONCRETE COVER DEGRADATION UNDER REINFORCEMENT CORROSION

Kseniya YURKOVA [a] and Tomasz KRYKOWSKI [b*]

[a] PhD; Faculty of Civil Engineering, Częstochowa University of Technology, ul. Dąbrowskiego 69, Częstochowa, Poland
ORCID: 0000-0002-8012-9466

[b] PhD, Associate Prof.; Faculty of Civil Engineering, Silesian University of Technology, ul. Akademicka 5, Gliwice, Poland
ORCID: 0000-0002-7294-1788

*Corresponding author. E-mail address: *tomasz.krykowski@polsl.pl*

Received: 28.04.2023; Revised: 26.05.2023; Accepted: 27.06.2023

Abstract

The paper presents a comparative analysis of the application of two nonlocal gradient-formulated models to evaluate the concrete cover degradation time. Calculations were made taking into account the increase in the volume of the steel ring around the perimeter of the reinforcement bar. The results of the calculations were compared with the results of experimental studies published in the literature and with the elastic-plastic model based on the Menetrey-Willam surface, in which the objectivity of the obtained results depends on the fracture energy. In addition, the paper compares solutions using different contact models and cohesion models.

Keywords: **Corrosion; FEM; Gradient methods; Plasticity; Cover degradation.**

1. INTRODUCTION

Modelling the damage time of the concrete cover is an important problem in estimating the durability of reinforced concrete elements. There have been many papers related to the assessment of this issue. Classic papers based on the analytical model of a thick-walled cylinder can be mentioned here [1, 2, 3], and a comprehensive review of the paper can be found in [4].

The use of computer methods allowed for a more detailed description of the problem, among others, including in the calculations additional fields related to the mass transport of aggressive substances, moisture, and heat [5], assuming an uneven and time-varying distribution of corrosion products on the circumference of the reinforcement [6, 7, 8, 9, 10, 11, 12, 13], or the description of contact steel concrete [14].

The consequence of the implementation of computational methods was the use of advanced concrete models: elastic-plastic regularized with cracking energy [15, 16] implemented in the papers [17, 10, 18, 19, 20, 21]. Elastic models with degradation, an example of which is the gradient model used in corrosion problems [22]. And finally other – often very complex – network, mesoscale, microplane, and xfem models are presented, among others, in the papers [23, 24, 25, 26, 27, 28].

In this paper, the possibility of using nonlocal gradient microplane models presented in [29] and [30] for the estimation of the cover cracking time in reinforcement corrosion was analysed. The calculations took into account the issues of contact and cohesion at the interface between reinforcement steel and concrete. The results of the calculations were compared with the results obtained on the basis of experimental tests and the results obtained for the elastic-plastic Menetrey-Willam model with fracture and hardening and softening that depend on the fracture energy.

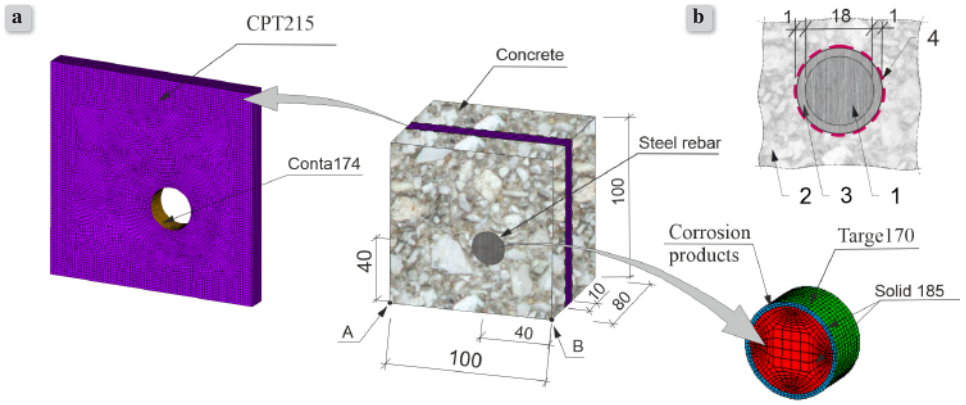


Figure 1.
Model of the test element subject to accelerated reinforcement corrosion: a) FEM model; b) steel-concrete contact zone model, description in the text

2. MODELS AND METHODS OF ANALYSIS

In the paper, calculations of the propagation of damage in the concrete cover of a test reinforced concrete element subjected to reinforcement corrosion were made. The results were taken as average values from the tests presented in the paper [9], where the test sample 100x100x80 mm^3 with an eccentrically placed reinforcing bar with a diameter of 20 mm was subjected to accelerated corrosion, Fig. 1.

The paper analyses the propagation of damage in the cover of a reinforced concrete element with the use of nonlocal gradient material models. In the calculations, two gradient models of concrete, the elastic damage microplane model (EDM) [29] and the coupled damage plasticity microplane model (CDPM) [30] were used. Due to the highly time-consuming calculations, a fragment of the test reinforced concrete element with a thickness of 10 mm was analysed. The plain strain condition was enforced by the applied boundary conditions. The division of the test element in the plane into finite elements with a length of 1.2 mm was assumed. In the longitudinal direction, the sample was divided into eight finite elements, Fig. 1. The impact of corrosion products on the concrete cover was captured by introducing the equivalent rate tensor of the volumetric strain [9]. It was assumed that the mechanical effects of the interaction could be represented using a steel ring to which the coordinate of increment of the volume strain tensor would be applied. The steel-concrete bonds were mapped using contact elements and a cohesion model. The diagram of the division of the test element into finite elements together with the concept of modelling corrosion effects in the form of a steel ring is shown in Fig. 1b, where the following indications have been adopted: 1) reinforcing steel, 2) concrete, 3) steel ring, 4) contact.

3. MATHEMATICAL MODEL

3.1. Introduction

The analyses of concrete cover cracking were performed using microplane models [31, 32]

$$\sigma_V^e = \frac{\partial \Psi^{mac}}{\partial \varepsilon_V}, \qquad \boldsymbol{\sigma}_D^e = \frac{\partial \Psi^{mac}}{\partial \boldsymbol{\varepsilon}_D},$$
$$\Psi^{mac} = \frac{3}{4\pi}\int_\Omega \Psi^{mic} d\Omega, \tag{1}$$

$$\Psi^{mic} = \left(1 - d^{mic}\right)\left(\frac{1}{2}K^{mic}(\varepsilon_V^e)^2 + G^{mic}\boldsymbol{\varepsilon}_D^e : \boldsymbol{\varepsilon}_D^e\right),$$
$$\varepsilon_V^e = \frac{\mathrm{Tr}(\boldsymbol{\varepsilon}^e)}{3}, \qquad \boldsymbol{\varepsilon}_D^e = \mathrm{dev}(\boldsymbol{\varepsilon}^e), \tag{2}$$

where σ_V^e is the effective volumetric stress, σ_D^e is the deviator of effective stress tensor, $\boldsymbol{\varepsilon}$ is the strain tensor, d^{mic} is the damage parameter assigned to the microplane, $K^{mic} = 3K$ and $G^{mic} = G$ are elastic material parameters related to the microplane, K and G are the bulk modulus and Kirchhoff modulus, respectively, ε_V^e is the elastic part of the microplane volumetric strain, ε_D^e is elastic part of the deviator of the microplane strain tensor, Ψ^{mac} and Ψ^{mic} are respectively macroscopic and microscopic Helmholtz free energy.

The mesh-independent solution was guaranteed by the formulation of a gradient (nonlocal) model [29, 30].

3.2. Elastic damage model (EDM)

The EDM model is formulated in [29] and in the documentation of the ANSYS software [33]. The damage surface and the evolution equation of the damage parameter are described by the following relations:

- Damage surface (modified Mises surface).

The equivalent strain corresponding to the microplane is determined in accordance with the relationship used, among others, in the papers of [34, 29, 35 and 36].

$$\eta^{mic} = k_0 I_1 + \sqrt{(k_1 I_1)^2 + k_2 J_2}, \tag{3}$$

$$k = \frac{f_c}{f_t}, \quad k_0 = k_1 = \frac{k-1}{2k(1-2\nu)}, \quad k_2 = \frac{3}{k(1+\nu)^2}, \tag{4}$$

where k_0, k_1, k_2 are material parameters.

- Equation of the evolution of the damage parameter

The evolution equation of the damage parameter was proposed in the form of an exponential relationship [29, 34, 35, 36]

$$d^{mic} = 1 - d^{mic,\gamma},$$

$$d^{mic,\gamma} = \frac{\gamma_0^{mic}}{\gamma^{mic}}\left[1 - \alpha^{mic} + \alpha^{mic}\exp(\beta^{mic}(\gamma_0^{mic} - \gamma^{mic}))\right] \tag{5}$$

$$\gamma^{mic}(t) = \max_{\tau \le t}\left(\gamma_0^{mic}, \eta^{mic}(\tau)\right), \qquad \gamma_0^{mic} = w_\gamma \frac{f_t}{E}. \tag{6}$$

where γ^{mic} is a history variable representing the highest value of the equivalent strain in the material's history, α^{mic} is the parameter determining the maximum allowable value of material degradation, β^{mic} is the parameter determining the rate of evolution of damage, γ_0^{mic} is the damage threshold that characterizes the start point of the equivalent strain, $w_\gamma \in (0,1)$ is the scaling factor.

3.3. Coupled plastic damage model (CPDM)

The constitutive relationships in the CPDM model, after considering the decomposition of the strain tensor into elastic and plastic parts, will take the form [30]

$$\begin{aligned} \sigma_V^e &= 3K\left(\varepsilon_V - \varepsilon_V^{pl}\right), \\ \boldsymbol{\sigma}_D^e &= 2G\left(\boldsymbol{\varepsilon}_D - \boldsymbol{\varepsilon}_D^{pl}\right), \end{aligned} \tag{7}$$

$$\begin{aligned} \varepsilon_V &= \varepsilon_V^e + \varepsilon_V^{pl}, \qquad \dot{\varepsilon}_V^{pl} = \dot{\lambda}\frac{\partial f^{mic}}{\sigma_V^e}, \\ \boldsymbol{\varepsilon}_D &= \boldsymbol{\varepsilon}_D^e + \boldsymbol{\varepsilon}_D^{pl}, \qquad \dot{\boldsymbol{\varepsilon}}_D^{pl} = \dot{\lambda}\frac{\partial f^{mic}}{\boldsymbol{\sigma}_D^e}, \end{aligned} \tag{8}$$

where ε_V is the volumetric microplane strain, ε_V^{pl} is the volumetric microplane plastic strain, $\boldsymbol{\varepsilon}_D$ is the deviator of the microplane strain tensor, $\boldsymbol{\varepsilon}_D^{pl}$ is the plastic part of the deviator of the microplane strain tensor.

The microplane yield surfaces f^{mic} and the component cap surfaces take the form:

- Microplane yield surface f^{mic}

$$f^{mic} = \frac{3}{2}\boldsymbol{\sigma}_D^e : \boldsymbol{\sigma}_D^e - g_1^2 g_c g_t, \tag{9}$$

where g_1 is the Drucker-Prager yield function with hardening, g_c and g_t are the compression and tension cap functions.

- The Drucker-Prager yield function,

$$\begin{aligned} g_1(\sigma_V^e, \kappa) &= \sigma_0 - \alpha_f \sigma_V^e + f_h(\kappa), \\ f_h(\kappa) &= D\kappa, \end{aligned} \tag{10}$$

where σ_0 is the initial yield stress, f_h is a hardening function, D is a hardening material constant, α_f is a friction coefficient, κ is a hardening variable.

- The compression cap function g_c,

$$g_c(\sigma_V^e, \kappa) = 1 - \frac{H_c(\sigma_V^c - \sigma_V^e)(\sigma_V^c - \sigma_V^e)^2}{X^2}, \quad X = R g_1(\sigma_V^c), \tag{11}$$

where σ_V^c is the abscissa of the intersection point between g_1 and g_c, R is the ratio between the major and minor axes of the cap, H_c is the Heaviside step function.

- The tension cap function g_t,

$$\begin{aligned} g_t(\sigma_V^e, \kappa) &= 1 - \frac{H_t(\sigma_V^e - \sigma_V^T)(\sigma_V^e - \sigma_V^T)^2}{(T - \sigma_V^T)^2}, \\ T &= T_0 + R_T f_h, \qquad T_0 = \frac{1}{3} f_t, \end{aligned} \tag{12}$$

where σ_V^T is the abscissa of the intersection point between g_1 and g_t, R_T is the tension cap hardening constant, H_t is the Heaviside step function.

- Equation of damage parameter evolution

$$\begin{aligned} d^{mic} &= 1 - (1 - d_c^{mic})(1 - r_w d_t^{mic}), \\ r_w &= \frac{\sum_{I=1}^{3}\langle \varepsilon^I \rangle}{\sum_{I=1}^{3}|\varepsilon^I|} \end{aligned} \tag{13}$$

where $\langle \varepsilon^I \rangle$ is the McAulay bracket, d^{mic} is the damage parameter assigned to the microplane, d_c^{mic} is part of the compression damage parameter, d_t^{mic} is part of the tension damage parameter.

3.4. Modelling of steel-corrosion products-concrete interactions

3.4.1. Model of corrosion interactions

Studies that analysed the discrepancies of the calculated results obtained for the elastic-plastic hardening and softening model, different types of contact, and different variants of corrosion product modelling were conducted and presented, among others, in [21]. In this paper, it was assumed that the impact of corrosion products on the concrete cover can be described by imposing a deformation field on a steel ring on the perimeter of the reinforcement bar. According to [9] the evolution tensor of the corrosion volumetric strains rate was accepted in the form

$$\dot{\varepsilon}^{V}_{\alpha\beta} = \dot{\varepsilon}^{V}\delta_{\alpha\beta} = \frac{(1-\beta)(\alpha^{-1}\vartheta - 1)k_{comp}I}{\eta\varrho_{Fe^{2+}}V_0}\delta_{\alpha\beta}, \quad \alpha,\beta = 1,2, \quad k_{comp} = \chi k_{eff}, \quad \eta = \begin{cases} 3\beta + 2(1-\beta), & t \le t_{cr} \\ 2, & t > t_{cr} \end{cases}, \tag{14}$$

$$\beta = \begin{cases} 1, & t \le t_0 \\ \dfrac{t_{cr} - t}{t_{cr} - t_0}, & t_0 \le t \le t_{cr}, \\ 0, & t > t_{cr} \end{cases} \tag{15}$$

where β is a parameter of the intensity of corrosion products interaction with the cover of concrete; α, ϑ are parameters depending on the composition of corrosion products; k_{comp} and k_{eff} are respectively the calculated and effective electrochemical equivalent of iron; I is the corrosion current; t_{cr} is the critical time, while V_0 is the initial volume of the analysed area in which the volume of corrosion products increases.

3.4.2. Model of contact and cohesive interactions

Contact interactions were analysed according to the algorithm presented in the paper [21]. The contact area of steel and concrete was mapped using contact elements in which the Coulomb friction model was included along with the possibility of separation of the contact surface and the cohesion model, which were implemented in the APDL language [33]. The paper analysed the options of contact interactions: rigid contact (B), characterised by the lack of slippage and separation; flexible contact (NSS), allowing contact slippage in the tangential direction; standard contact (S), allowing contact slippage and separation of contact surfaces; and the cohesion model (CZM), allowing for the description of contact degradation of contact surfaces.

The cohesive degradation of the steel-concrete contact zone was explained using a bilinear cohesive model of the material [14], depending on the contact normal stresses σ_n and tangential stresses τ_t. The cohesion model used in the calculations carried out in the paper is applied simultaneously with the Coulomb friction model (the shear stress is the maximum value determined on the basis of both models) [21].

4. COMPUTATIONAL MODEL

4.1. Introduction

The computer simulation was carried out using the parameters adopted in the paper [9] in the ANSYS software. It was accepted that the corrosion products are a mixture of iron oxides $Fe(OH)_2$ and $Fe(OH)_3$, the effective electrochemical equivalent of iron k_{eff}=0.006271 (g/μA·year), filling time of porous zone t_0 = 13 h, critical time t_{cr} = 53.83 h.

The value of increments of corrosion volumetric strains was determined for the averaged function of the corrosion current intensity [9]. The course in the changes in the increments of volumetric strains as a function of the averaged current intensity for the entire cross-section of the reinforcing bar and the parameter χ =1 is shown in Fig. 2 (calculations were carried out assuming the parameter χ =0.4).

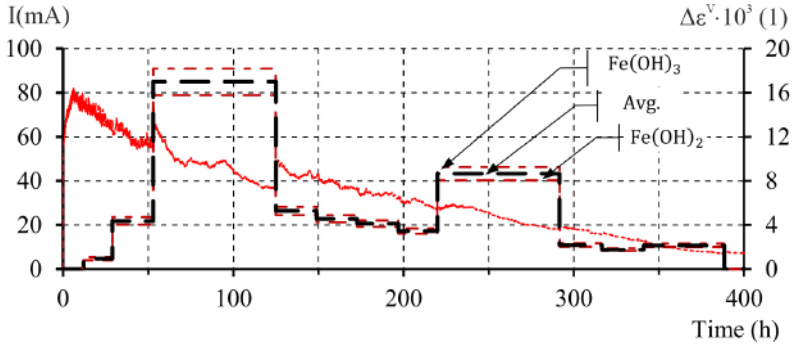


Figure 2.
Functions of the intensity of the current and equivalent increments of volumetric strains in the plane perpendicular to the reinforcing bar axis, Δε (description in the text)

In the FEM model, the elements of ANSYS software CPT215 were used for the concrete modelling and SOLID185 for the reinforcement bar modelling. Contact interactions were modelled using elements TARGE170 and CONTA174. The computational analysis also considered the issue of cohesion, which was associated with the contact elements in the computational system. The corrosive effects were included considering the increases in corrosive volumetric strains in the steel ring, Fig. 1b. Calculations were made for the cover described with EDM and CDPM materials in a nonlocal gradient formulation. For steel, the Huber-Mises-Hencky elastic-plastic model without hardening was assumed. The initial elastic material parameters of the concrete along with the basic strength parameters of the steel are summarized in Table 1 and Table 2, respectively.

Table 1.
Initial elastic and strength material parameters of concrete

Description	Value
Modulus of elasticity, E (GPa)	38.28
Poisson's ratio, ν (–)	0.2
Uniaxial tensile strength, f_t (MPa)	3.99
Uniaxial compressive strength, f_c (MPa)	56.4
Biaxial compressive strength, $f_{bc}=1.15\ f_c$ (MPa)	64.86

Table 2.
Initial elastic and strength material parameters of steel

Description	Value
Modulus of elasticity, E_s (GPa)	200
Poisson's ratio, ν_s (1)	0.3
Yield strength, f_y (MPa)	235

The determination of inelastic parameters requires experimental research. Due to the impossibility of making such tests, the inelastic parameters of concrete were determined on the basis of empirical relationships characterising the parameters of the model as well as numerical tests of cyclic loading and unloading of homogeneous elements in compression/tension, Fig. 3b and nonhomogeneous tensile test elements with a notch, Fig. 3a. Numerical tests were related to the calculations made using the elastic-plastic model of the material with hardening/softening dependent on the fracture energy Menetrey-Willam (MW) model with HSD2 implemented in the ANSYS software [21, 33]. The material parameters of the model are listed in Table 1 and Table 3. The mesh of the test elements was densified in the stress concentration region, Fig. 3a.

Table 3.
Inelastic parameters of the MW model with HSD2 [21]

Description	Value	Description	Value
Fracture energy, G_{ft} (N/m)	151	Ω_{ci} (1)*)	0.33
Dilation angle, ψ (Deg)	20	Ω_{cu} (1)*)	0.85
κ_{cm} (1)*)	0.00151	Ω_{cr} (1)*)	0.2
κ_{cu} (1)*)	0.00175	Ω_{tr} (1)*)	0.1

*) parameter characterizing the hardening/softening curve of the HSD2 model under compression and tension

4.2. Parameters of the material models

4.2.1. Gradient elastic damage model

The formulation of the gradient elastic damage model (EDM) requires the definition of 7 parameters (plus E and ν). The first three k_0, k_1, k_2 and the

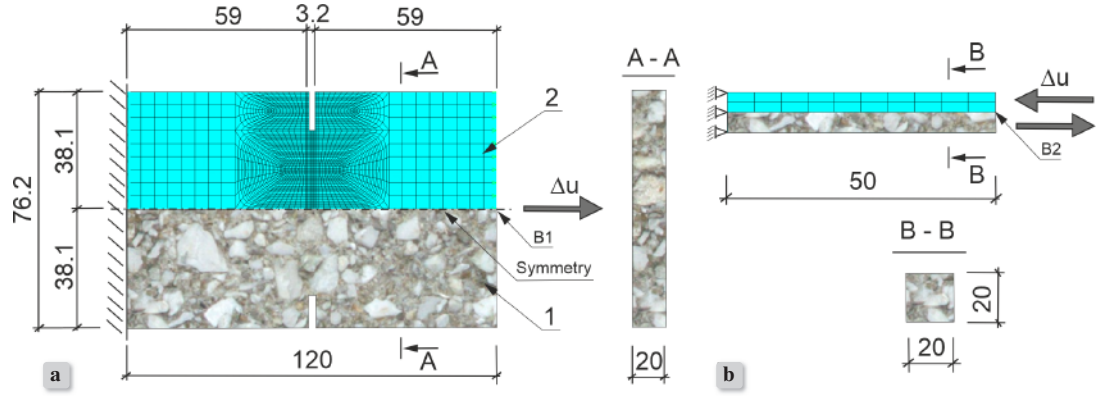


Figure 3.
Test model: a) notched tensile sample and b) cyclically compressed sample

parameter defining the damage threshold γ_0^{mic} are described by the empirical formulas (4), (6). In the analysis the scaling factor $w_\gamma = 0.9$. The parameter describing the degradation function β^{mic} and the gradient parameter c [35], [36] were determined based on the tests of the notched sample shown in Fig. 3a. The value describing the acceptable degradation of the material $\alpha^{mic} = 0.96$ was adopted at the stage of the initial loading tests of the sample.

In the element, according to Fig. 3a, the displacement of the element edge $\Delta u = 0.2$ mm was induced, assuming variable parameters characterizing the shape of the degradation function β^{mic}. The results of the tensile test characterizing the response of the test element are presented in Fig. 4a, where the following denotations were assumed: $\beta^{mic} = 50$ (F1), $\beta^{mic} = 100$ (F2), $\beta^{mic} = 300$ (F3) for c=5 mm^2 and $\beta^{mic} = 50$ (F5), $\beta^{mic} = 100$ (F6), $\beta^{mic} = 300$ (F7) for c=8 mm^2, model MW with HSD2 (F4). The β^{mic} parameter was finally assumed by iterative analysis of the response of the notched tensile sample, the deformation map for the EDM model, as well as by analysing the results and the convergence of the solution of the test sample analysed in the paper, in which reinforcement corrosion occurs. For the purposes of further calculations, the values $\beta^{mic} = 100$, c = 8 mm^2 (model F6) were assumed, for which the calculations in the test sample were also characterized by high stability.

4.2.2. Gradient coupled damage-plasticity microplane model

In the case of an elastic-plastic gradient material model with degradation (CDPM), it is required to define 13 material parameters (plus E and ν). The parameters of the CDPM model σ_V^C and R can be assumed based on the empirical relationships [37, 38, 30]

$$\sigma_V^C = -\frac{2}{3} f_{bc}, \qquad R = \frac{X_0}{f_1(\sigma_V^C)}, \tag{16}$$

where f_{bc} is the strength of the concrete in biaxial compression.

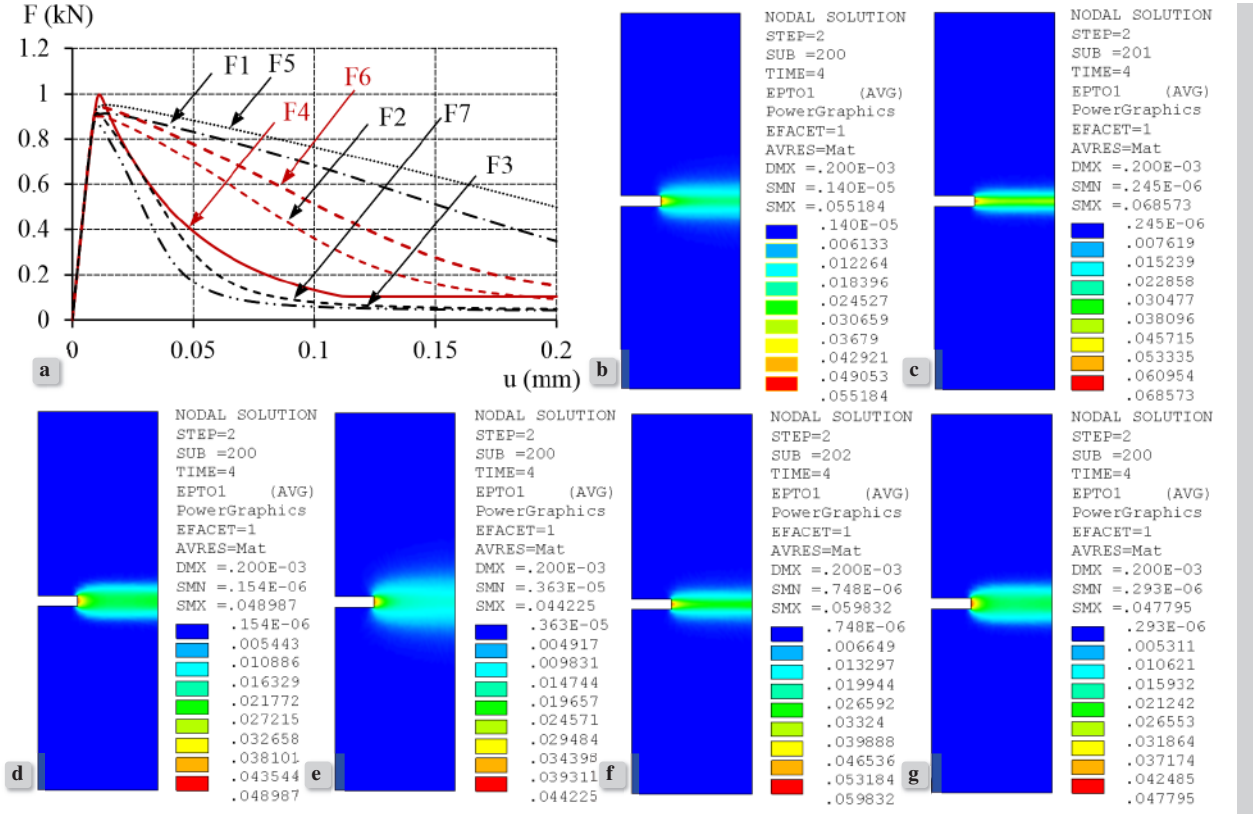


Figure 4.
Response of the system and maps of principal tensile strains ε_1 (model EDM, variables c, β): a) response of the system; b) c = 5 mm^2, β = 50; c) c = 5 mm^2, β = 100; d) c = 5 mm^2, β = 300, e) c = 8 mm^2, β = 50; f) c = 8 mm^2, β = 100; g) c = 8 mm^2, β = 300

Other parameters require computational tests. In the first stage, a cyclic axial compression test was performed, which allowed the determination of the parameters D, β_c, γ_{c0}. In the next one, the axial stretching of the inhomogeneous notched sample was analysed which allowed the determination of the values R_T, β_t, γ_{t0}, as well as the gradient parameters c and m.

In the first stage of the calculations, in the cyclic compression and tensile test of the unnotched concrete sample, Fig. 3b, the parameters D, β_c, γ_{c0} were determined. In the absence of experimental studies, the parameters were accepted as starting values for the calculations [30]

$$R_T = 1, \qquad \beta_t = 1.5\beta_c, \qquad \gamma_{t0} = w_\gamma \frac{f_t}{E_0}, \qquad w_\gamma = 0.9, \qquad m = 2.5. \tag{17}$$

Computer calculations of the cyclic compression test were made for the material parameters listed in Table 4. Table 5 presents the variable test parameters for which the response of the system was tested to select its best values.

The calculation results obtained for the variable (modified) material parameters β_t, β_c, D, γ_{c0} are shown in Fig. 5 where the following indications have been introduced: a) M1, M2, M3 are the results of the calculations for changing parameters β_t and β_c acc. to relation (18); b) M4, M5 are the results of the calculation for the change parameter D; c) M6, M7, M8 are the results of the calculations obtained with the changing parameter γ_{c0} (other parameters were assumed according to Table 4). The test results obtained using the MW model with HSD2 are marked with the E2 index. The parameters obtained for the M7 test were assumed to be optimal: D=10000 MPa, $\beta_c = 2000$, $\beta_t = 2000$, $\gamma_{c0} = 0.0001$.

Table 4.
The material parameters of the CDPM model assumed in the cyclic compression test to determine the values D, β_c, γ_{c0}, [30]

Description of the variable	Value
Abscissa of the intersection point between the compression cap and the Drucker-Prager yield function, σ_V^c (MPa)	-50
The ratio between the major and minor axes of the cap, R (–)	2
Tension cap hardening constant, R_T (–)	1
Tension damage thresholds, $\gamma_{t0} \cdot 10^5$ (–)	9.38
Nonlocal interaction range parameter, c (–)	10
Over-nonlocal averaging parameter, m (–)	2.5
Tension damage evolution constant, β_t^* (–),	$\beta_t^*=1.5\,\beta_c^*$
Hardening material constant, D^* (MPa)	10000
Compression damage thresholds, γ_{c0}^* (–)	0.0001
Compression damage evolution constant, β_c^* (–)	1000

Table 5.
Variable material parameters of the CDPM model assumed for the cyclic compression test to determine the value D, β_c, γ_{c0}, [30]

Description	M1	M2	M3	M4	M5	M6	M7	M8
D/D^*	4	4	4	1	8	1	1	1
$\gamma_{c0}/\gamma_{c0}^*$	1	1	1	1	1	0.7	1	1.3
β_c / β_c^*	1	2	3	2	2	2	2	2
β_t/β_t^*	1	2	3	2	2	1.33	1.33	1.33

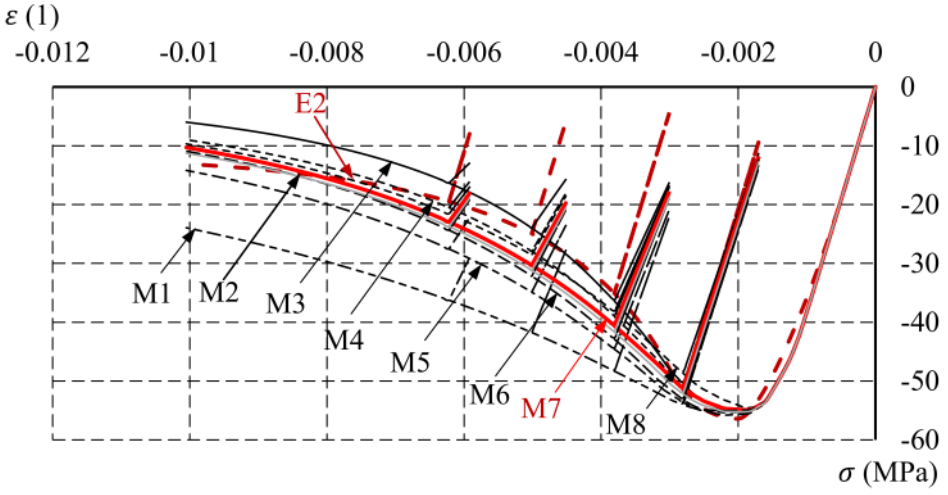


Figure 5.
Change of the σ-ε relationship in a cyclically compressed and tensiled sample (description in the text)

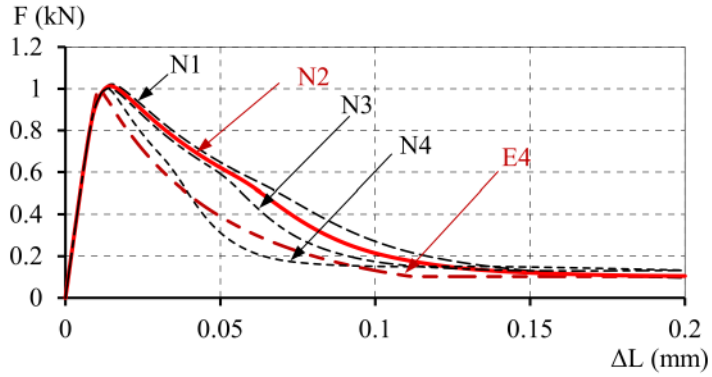


Figure 6.
Relationship between the force and displacement of the system with a variable value of the β_t parameter and the gradient parameter c (description in the text)

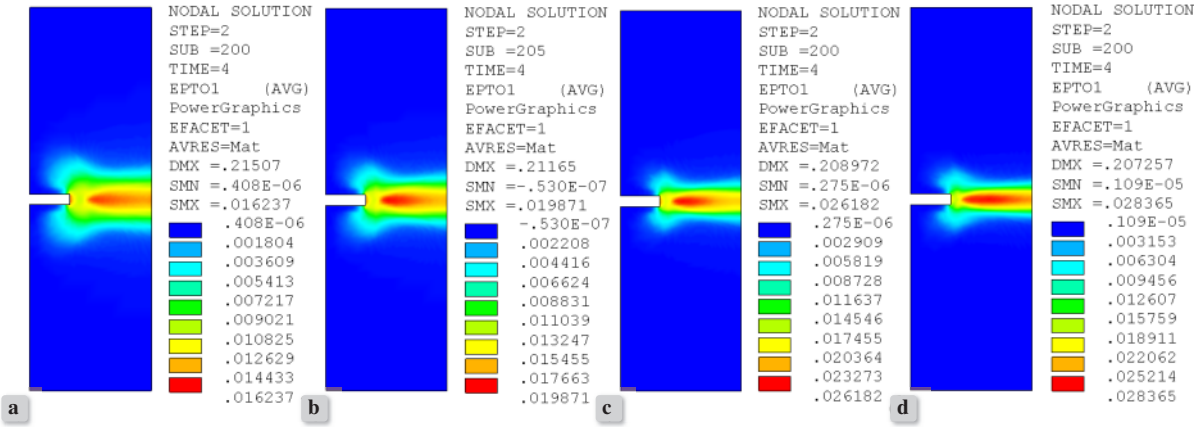


Figure 7.
Maps of the main tensile strains ε_1 of the notched element (CDPM model, variable parameters β_t and c): a) N1, $\beta_t = 2000$, c = 12; b) N2, $\beta_t = 2000$, c = 8; c) N3, $\beta_t = 2000$, c = 5; d) N4, $\beta_t = 3000$, c = 5

The second stage of selection of material parameters was performed for the test element with a notch, Fig. 3a. In the tensile test, the values of the parameters β_t and c, Table 6, were adopted while the remaining constants were assumed based on Table 4 and Table 5.

Table 6.
Variable material parameters of the CDPM model assumed for the tensile test to determine the values β_t and c [30]

Description	N1	N2	N3	N4
β_t	2000	2000	2000	3000
c (mm^2)	12	8	5	5

The values of the searched model parameters β_t and c, just as the first stage, were selected on the basis of the results of the tensile test of the notched sample. Graphs showing the system response in Fig. 3a as a result of forcing the displacement of the element edge are presented in Fig. 6 where N1-N4 are the test parameters of the model, E4 is the calculation result obtained using the MW model with HSD2.

In Fig. 6: N1-N4 are the test parameters of the model, and E4 is the calculation result obtained using the MW model with HSD2. The distribution of the principal tensile strains ε_1 of the notched test element in the CDPM model as a function of the parameter β_t (1) and c (mm^2): a) N1, $\beta_t = 2000$, c = 12; b) N2, $\beta_t = 2000$, c = 8; c) N3, $\beta_t = 2000$, c = 5; d) N4, $\beta_t = 3000$, c = 5, was shown in Fig. 7.

The parameter β_t and c were finally adopted in an iterative way by analysing the response of the notched tensile sample, the principal strain maps for the CDPM model shown in Fig. 7 as well as by analysing the results and convergence of the solution of the test sample analysed in the paper, where reinforcement corrosion occurred. For the purposes of further calculations, the values of the parameters $\beta_t = 2000$, c= 8 (mm^2) (model N2) were adopted, for which the calculations in the analysed test sample were also characterized by high stability.

4.2.3. Parameters of cohesion and contact models

The contact between the reinforcing steel and concrete was modelled for different contact models: a) rigid (B), b) no separation with slip (NSS), c) standard model with slip and separation (S), and d) cohesive model with degradation of the contact layer (CZM).

Material parameters of cohesion c_h, maximum allowable shear stresses τ_{max} and parameters related to normal stiffness K_n and tangent stiffness K_t were formulated as functions of the initial value K_n^0, which after a series of tests was taken as equal to $K_n^0 = 7.65 \cdot 10^8$ MN/m^3.

$$K_t^0 = \mu K_n^0, \qquad c_h = 0.05\sqrt{f_c}, \qquad \tau_{max} = 2.5\sqrt{f_c}, \quad (18)$$

where K_t^0 is the initial value of the tangent stiffness.

The material parameters assumed in the contact and cohesive models used in the calculations were defined in Table 7 and Table 8.

4.3. Calculation results

The calculation results for the EDM and CDPM models were compared with the mean displacement values obtained for the MW model with HSD2 and the solution obtained from the ATENA programme (elastic-plastic MW model with cracking [9]). The solution was also compared with the results of experimental studies of element edge displacements and the width of the crack, published in the paper [9]. The variants of materials and types of contact elements analysed in the paper are presented in Table 9.

In Table 9, the models used are marked with the first letter of the model name and the number that identifies the type of contact. The results of experimental calculations [9] are marked with the symbols: a) EX1 for the measured displacements, and b) EX2 for the values of the measured crack widths. The average calculation results obtained from the ATENA software for the rigid contact between steel and concrete are marked with the A index.

Table 7.
Contact model parameters: bonded, no separation with sliding, CZM, standard

Parameter	Value			
Coefficient of friction, μ (1)	1.0	0.2	0.2	0.2
Cohesion coefficient, c_h(MPa)	0.0	0.375	0.375	0.375
Normal contact stiffness, K_n/K_n^0	1.0	1.0	1.0	1.0
Tangent contact stiffness, K_t/K_t^0	1.0	2.0	5.0	5.0
Maximum allowable shear stress, τ_{max} (MPa)	1E20	18.77	18.77	18.77
Contact Type	B	NSS	CZM	S

Table 8.
Supplementary parameters of the cohesive model (CZM)

Parameter	Value
Maximum normal contact stress, σ_{max} (MPa)	3.99
Critical crack energy in the normal direction, G_{cn} (N/m)	151
Maximum tangential contact stress, $\tau_{t,max}$ (MPa)	2.26
Critical fracture energy in the tangential direction, G_{ct} (N/m)	113
Artificial damping parameter, η (1)	0.0001

Table 9.
List of materials and contact models analysed in the paper, along with denotations

Contact Type	MW with HSD2	EDM	CDPM
B	M1	E1	C1
NSS	M2	E2	C2
S	M3	E3	C3
CZM	M4	E4	C4

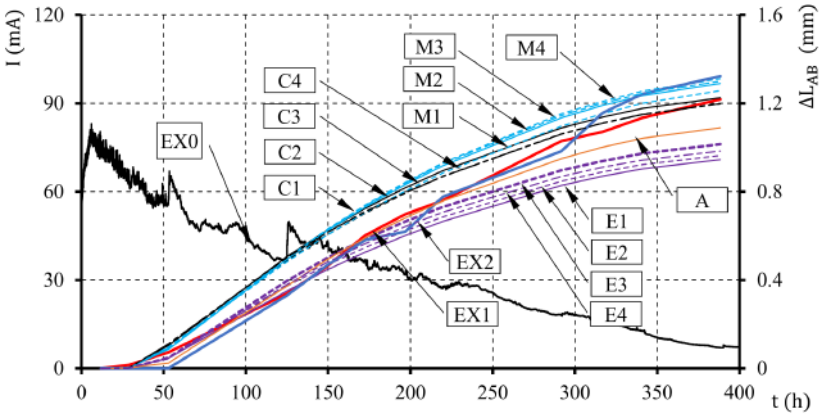


Figure 8.
The evolution of changes in the elongation of the edges of elements of reinforced concrete samples ΔL_{AB} as a result of reinforcement corrosion/calculation model (cf. Fig. 1)

The results of the calculations of displacement of the edge of element ΔL_{AB}, Fig. 1a by using the EDM and CDPM gradient models that are available in the ANSYS program, were presented graphically together with the comparative calculations and the results of the experimental tests in Fig. 8. The notation placed in the figure was explained in Table 9. The results of the experimental tests are marked with the following symbols: EX0 is the course of the change in the average value of the current intensity [9], EX1 is the course of the change of the averaged function of the edge displacements [9], EX2 is the course of the change in the average function of the width of the crack in the element [9]. The average results obtained using FEM from the ATENA software, assuming a rigid contact between steel and concrete, are marked with index A.

The analysis of the research results shows high compatibility of the results obtained using MW models with HSD2 and those obtained using the nonlocal gradient CDPM model. These results also show compliance with the final values of the crack width and displacements of the edges of the element. However, reference to the results of experimental tests is for illustrative purposes only, because obtaining these test results is subject to specific uncertainties related to the nature of the reinforcement corrosion processes. The method of transferring the results of experimental research assumptions to computer calculations is also characterized by uncertainty (uncertain parameter of the intensity of the impact of corrosion products χ). The results obtained using the ATENA software for the MW model with cracking, included in the paper for comparison, give lower displacement values, although it can be seen that the shape of the curve describing the history of displacements is similar to the previously obtained results. The mentioned model was additionally calculated for a coarser mesh of finite elements.

However, a strong deviation (about 30%) of the results obtained using the EDM gradient model from the results obtained with the MW models with HSD2 and CDPM as well as from the results obtained with the ATENA software [9] is very characteristic.

The results of the calculation (approximately) at the end of the time step t = 388 h for both the analysed EDM and CDPM models are compared in Table 10. The reference value was the result of the experiment included in the paper [9]. The calculations were made according to the dependencies.

$$|\Delta L_{AB}| = \left|L_{AB}^{EX} - L_{AB}^{i}\right|,$$
$$\left|\Delta L_{AB}^{\%}\right| = \frac{\left|L_{AB}^{EX} - L_{AB}^{i}\right|}{(L_{AB}^{EX} - L_{AB0})}, \quad (19)$$

where L_{AB}^{EX} is the length of the element edge after the time t = 388 h of forcing the corrosion of the reinforcement obtained as a result of experimental tests, L_{AB1}^{i} is the length of the element obtained using the compared model, L_{AB0} is the dimension of the edge unloaded.

In addition, graphic images of the main tensile strains for the following models are presented: a) CDPM in Fig. 9, b) EDM in Fig. 10, c) MW with HSD2 in Fig. 11.

Table 10.
Comparison of the calculation results and the percentage deviation from the results obtained for the MW model with HSD2

Model	L_{AB} (mm)	$\lvert\Delta L_{AB}\rvert$ (mm)	$\lvert\Delta L_{AB}^{\%}\rvert$(%)
EX1	101.22	-	-
EDM E1	100.94	0.27	29
EDM E2	100.96	0.25	26
EDM E3	101.01	0.20	20
EDM E4	100.98	0.23	24
CDPM C1	101.22	0.01	1
CDPM C2	101.20	0.02	2
CDPM C3	101.20	0.02	2
CDPM C4	101.20	0.02	2
MW M1	101.29	0.07	6
MW M2	101.26	0.04	3
MW M3	101.31	0.09	7
MW M4	101.30	0.08	6

5. SUMMARY

The results obtained from the calculations well reflect the behaviour of the reinforced concrete covers under the conditions of accelerated reinforcement corrosion. The convergence of the results of calculations aimed at determining the displacements of the edge of the reinforced concrete element subjected to reinforcement corrosion in the case of the MW models with HSD2 and CDPM is high (the deviation of the results is approximately 5%). The use of gradient models allows for obtaining fully mesh-independent (objective) results of computer calculations; however, it is very computationally expensive and requires a dense FE mesh. In the test calculations analyzed in the paper, in the case of irregular finite elements, the solution did not converge. Convergence problems were also conditioned by the type of contact used. In the case of contact B, the NSS solution converged very well. In the case of S-type and CZM contact, a high dependence of the stability of the solution on the proportion of the dimensions of the finite elements could be observed,

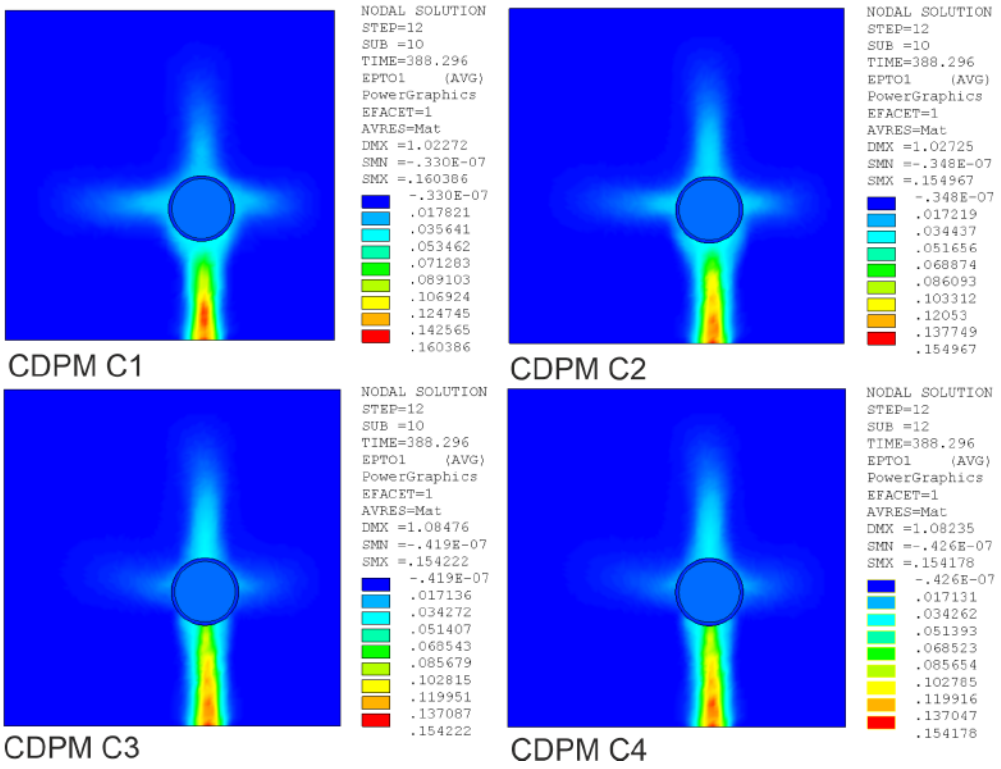


Figure 9.
Maps of total and principal strains, ε_1, with the CDPM gradient model, time t=388 h

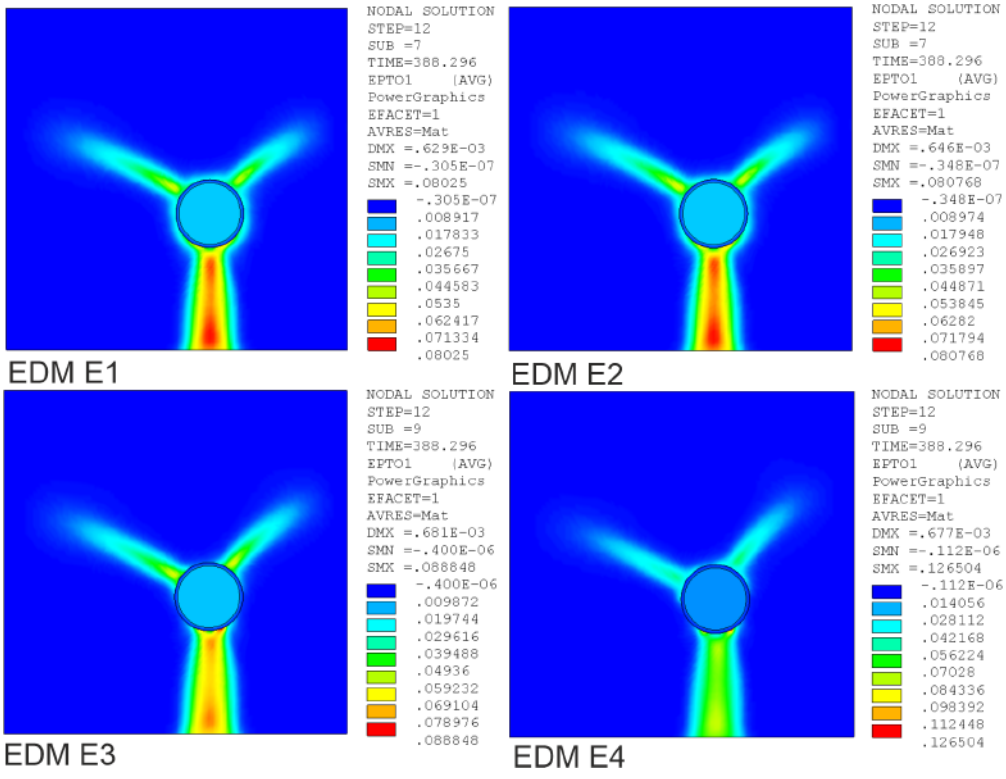


Figure 10.
Maps of total and principal strains, ε_1, with the EDM gradient model, time t=388 h

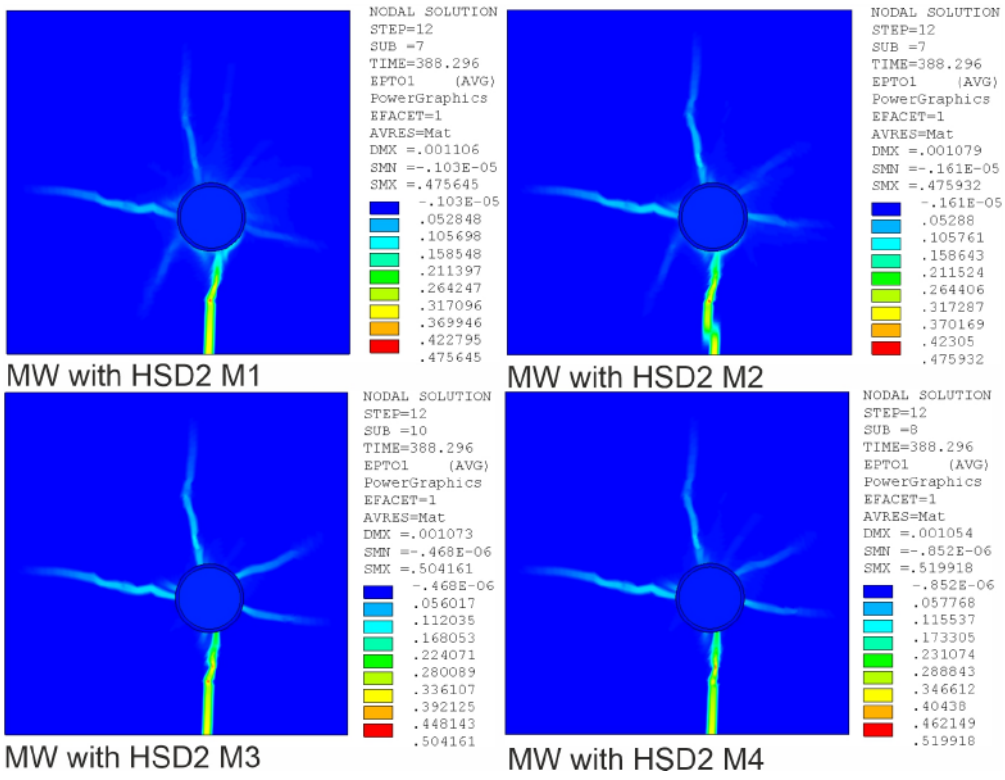


Figure 11.
Maps of the total and principal strains, ε_1, model MW with HSD2, time t=388 h

both in the case of the EDM and CDPM models. The deviation of the solution obtained using the EDM gradient model from the results obtained for the MW and CDPM models may result from the selection of the gradient parameter c.

In the case of the EDM model (as in the CDPM), the value of the gradient parameter c=8 mm^2 was assumed. The adoption of lower values of the gradient parameter allowed for a more precise map of total deformations (cracks), but it required the use of a denser FE mesh, which resulted in a significant increase in calculation time. In the EDM model, the use of higher values of the gradient parameter c did not represent the principal maps of the total tensile strains in an acceptable manner. In the CDPM model, the influence of the gradient parameter on the values of the calculation results was less than in the EDM model.

From the point of view of the damage pattern distribution the results from CDPM and MW with HSD2 models are very close to the damage pattern. From the applicability point of view (because of the rate of the solution of the problem) the MW with HSD2 model is most promising.

ACKNOWLEDGEMENTS

This research project was financially supported by the National Centre for Research and Development, NCBR, Poland, the competition for research projects with the participation of scientists from Belarus entitled “Solidarity with scientists”, Modelling the durability and degradation of reinforced concrete elements in conditions of reinforcement corrosion.

LATIN SYMBOLS

c – nonlocal interaction range parameter,

c_h – cohesion coefficient,

D – hardening material constant,

d^{mic} – damage parameter assigned to the microplane,

d_c^{mic} – part of the compression damage parameter,

d_t^{mic} – part of the tension damage parameter,

E, E_s – Young’s modulus of concrete/steel,

f_{bc} – biaxial compressive strength,

f_c – uniaxial compressive strength,

f_h – hardening function,

f_t – uniaxial tensile strength,

f_y – yield strength,

f^{mic} – microplane yield function,

G – Kirchhoff modulus,

G_{cn} – critical crack energy in the normal direction,

G_{ct} – critical fracture energy in the tangential direction,

G_{ft} – fracture energy,

g_1 – Drucker-Prager yield function with hardening,

g_c – compression cap function,

G^{mic} – elastic material parameter related to the microplane,

g_t – tension cap function,

H_c,H_t – Heaviside step functions.

I – corrosion current,

I_1 – first invariant of strain tensor,

J_2 – second invariant of the deviatoric part of the strain tensor,

K – bulk modulus,

k_0 – microplane equivalent strain parameter,

k_1 – microplane equivalent strain parameter,

k_2 – microplane equivalent strain parameter,

k_{comp} – the calculated electrochemical equivalent of iron,

k_{eff} – the effective electrochemical equivalent of iron,

K_n – normal contact stiffness,

K_t – tangent contact stiffness,

K^{mic} – elastic material parameter related to the microplane,

m – over-nonlocal averaging parameter

R – the ratio between the major and minor axes of the cap,

R_T – tension cap hardening constant,

t_0 – filling time of porous zone,

t_{cr} – critical time,

T_0 – the initial intersection of the cap with the volumetric axis,

T – intersection of the cap with the volumetric axis,

V_0 – the initial volume of the analysed area in which the volume of corrosion products increases,

w_γ – scaling factor,

X – function yield function g_1 and R,

Greek SYMBOLS

α_f – friction coefficient,

α, ϑ – parameters depending on the composition of corrosion products,

α^{mic} –parameter determining the maximum allowable value of material degradation,

β – parameter of the intensity of corrosion products interaction with the cover of concrete,

β_c, β_t – compression/tension damage evolution constants,

β^{mic} – rate of damage evolution,

γ_{c0} – compression damage thresholds,

γ_{t0} – tension damage thresholds,

γ_0^{mic} – damage threshold,

γ^{mic} – variable representing the highest value of the equivalent strain in the material's history,

$\delta_{\alpha\beta}$ – Kronecker delta,

$\boldsymbol{\varepsilon}$ – is the strain tensor,

ε_V – volumetric microplane strain,

ε_V^{el} – volumetric microplane elastic strain,

$\boldsymbol{\varepsilon}_V^{pl}$ – volumetric microplane plastic strain,

$\boldsymbol{\varepsilon}_D$ – deviator of the microplane strain tensor,

$\boldsymbol{\varepsilon}_D^e$ – elastic part of the deviator of the microplane strain tensor,

$\boldsymbol{\varepsilon}_D^{pl}$ – plastic part of the deviator of the microplane strain tensor,

$\dot{\varepsilon}_{\alpha\beta}^V$ – component of evolution tensor of the corrosion volumetric strain rate,

η – artificial damping parameter,

η^{mic} – microplane equivalent strain,

κ – hardening variable,

κ_i, Ω_i – HSD2 hardening/softening curve parameters, i ≡ cm, cu, ci, cr, tr,

μ – coefficient of friction,

ν, ν_s – Poisson's ratio,

$\varrho_{Fe^{2+}}$ – steel ions density,

σ_0 – initial yield stress,

$\boldsymbol{\sigma}_D^e$ – deviator of effective stress,

σ_{max} – maximum normal contact stress,

σ_V^c – abscissa of the intersection point between g_1 and g_c,

σ_V^T – abscissa of the intersection point between g_1 and g_t,

σ_V^e – effective volumetric stress,

τ_{max} – maximum allowable shear stresses,

$\tau_{t,max}$ – maximum tangential contact stress,

χ – parameter of the intensity of the impact of corrosion products,

ψ – dilation angle,

ψ^{mac} – macroscopic Helmholtz free energy,

ψ^{mic} – microscopic Helmholtz free energy.

REFERENCES

[1] Liu, Y. (1996). Modeling the Time-to-Corrosion Cracking of the Cover Concrete in Chloride Contaminated Reinforced Concrete Structures (PhD thesis, Virginia Polytechnic Institute and State University), Blacksburg, VA, United States.

[2] Bazant, Z. P. (1979). Physical model for steel corrosion in concrete sea structures—application. *Journal of the Structural Division, ASCE, 105*(6), 1155–1166. https://doi.org/10.1061/JSDEAG.0005169.

[3] Pantazopoulou, S. J., & Papoulia, K. D. (2001). Modeling Cover-Cracking due to Reinforcement Corrosion in RC Structures. *Journal of Engineering Mechanics, 127*(4), 342–351. https://doi.org/10.1061/(ASCE)0733-9399(2001)127:4(342)

[4] Jamali, A., Angst, U., Adey, B., & Elsener, B. (2013). Modeling of corrosion-induced concrete cover cracking: A critical analysis. *Construction and Building Materials*, 42, 225–237. https://doi.org/10.1016/j.conbuildmat.2013.01.019.

[5] Martín-Pérez, B. (1999). Service Life Modelling of R.C. Highway Structures Exposed to Chlorides (PhD Thesis, University of Toronto), Toronto, Canada.

[6] Molina, F. J., Alonso, C., & Andrade, C. (1993). Cover cracking as a function of rebar corrosion: Part 2 - Numerical model. *Materials and Structures, 26*(9), 532–548. https://doi.org/10.1007/BF02472864.

[7] Ožbolt, Joško, Oršanic, F., Gojko, B., & Kušte, M. (2012). Modeling damage in concrete caused by corrosion of reinforcement: coupled 3D FE model. *International Journal of Fracture*, 178, 233–244. https://doi.org/10.1007/s10704-012-9774-3.

[8] Wieczorek, B., & Krykowski, T. (2017). Zastosowanie reguł mechaniki uszkodzeń do oceny wzrostu odkształceń korozyjnych w warstwie przejściowej (Application of damage mechanics rules to evaluate the growth of corrosive deformations in transition layer). *Ochrona Przed Korozją, 60*(1), 5–8. https://doi.org/10.15199/40.2017.1.1.

[9] Krykowski, T., Jaśniok, T., Recha, F., & Karolak, M. (2020). A Cracking Model for Reinforced Concrete Cover, Taking Account of the Accumulation of Corrosion Products in the ITZ Layer, and Including Computational and Experimental Verification. *Materials, 13*(23), 5375. h ttps://doi.org/10.3390/ma13235375.

[10] German, M., & Pamin, J. (2015). FEM simulations of cracking in RC beams due to corrosion progress. *Archives of Civil and Mechanical Engineering*. https://doi.org/10.1016/j.acme.2014.12.010.

[11] Pluciński, P. (2008). Numeryczna analiza efektów mechanicznych korozji stali zbrojeniowej w betonie (Numerical analysis of mechanical effects of rebar corrosion in concrete structures) (PhD thesis, Cracow University of Technology). Poland, Kraków.

[12] Cao, C., & Cheung, M. M. S. (2014). Non-uniform rust expansion for chloride-induced pitting corrosion in RC structures. *Construction and Building Materials*, 51, 75–81. https://doi.org/10.1016/j.conbuildmat.2013.10.042.

[13] Chauhan, A., & Sharma, U. K. (2021). Crack propagation in reinforced concrete exposed to non-uniform corrosion under real climate. *Engineering Fracture Mechanics*, 248, 107719. https://doi.org/10.1016/j.engfracmech.2021.107719.

[14] Alfano, G., & Crisfield, M. A. (2001). Finite element interface models for the delamination analysis of laminated composites: Mechanical and computational issues. *International Journal for Numerical Methods in Engineering, 50*(7). https://doi.org/10.1002/nme.93.

[15] Lubliner, J., Oliver, J., Oller, S., & Oñate, E. (1989). A plastic-damage model for concrete. *International Journal of Solids and Structures, 25*(3), 299–326. https://doi.org/10.1016/0020-7683(89)90050-4.

[16] Červenka, J., & Papanikolaou, V. K. (2008). Three dimensional combined fracture-plastic material model for concrete. *International Journal of Plasticity, 24*(12), 2192–2220. https://doi.org/10.1016/j.ijplas.2008.01.004.

[17] Dai, L., Long, D., & Wang, L. (2021). Meso-scale modeling of concrete cracking induced by 3D corrosion expansion of helical strands. *Computers and Structures*, 254, 106615. https://doi.org/10.1016/j.compstruc.2021.106615.

[18] Zhang, Y., & Su, R. K. L. (2020). Corner cracking model for non-uniform corrosion-caused deterioration of concrete covers. *Construction and Building Materials*, 234, 117410. https://doi.org/10.1016/j.conbuildmat.2019.117410.

[19] Su, R. K. L., & Zhang, Y. (2019). A novel elastic-body-rotation model for concrete cover spalling caused by non-uniform corrosion of reinforcement. *Construction and Building Materials*, 213, 549–560. https://doi.org/10.1016/j.conbuildmat.2019.04.096.

[20] Baji, H. (2020). Stochastic modelling of concrete cover cracking considering spatio-temporal variation of corrosion. *Cement and Concrete Research*, 133, 106081. https://doi.org/10.1016/j.cemconres.2020.106081.

[21] Yurkova, K., & Krykowski, T. (2022). Modelowanie powstawania produktów korozji zbrojenia i ich wpływu na uszkodzenie otuliny betonowej (Modeling of the formation of reinforcement corrosion products and their impact on damage of the concrete cover). *Inżynieria i Budownictwo, 78*(9–10), 410–413.

[22] Seetharam, S. C., Laloy, E., Jivkov, A., Yu, L., Phung, Q. T., Pham, N. P., Kursten, B., & Druyts, F. (2019). A mesoscale framework for analysis of corrosion induced damage of concrete. *Construction and Building Materials*, 216, 347–361. https://doi.org/10.1016/j.conbuildmat.2019.04.252.

[23] Šavija, B., Luković, M., Pacheco, J., & Schlangen, E. (2013). Cracking of the concrete cover due to reinforcement corrosion: A two-dimensional lattice model study. *Construction and Building Material*s, 44, 626–638. https://doi.org/10.1016/j.conbuildmat.2013.03.063.

[24] Nguyen, T. T. H., Bary, B., & De Larrard, T. (2015). Coupled carbonation-rust formation-damage modeling and simulation of steel corrosion in 3D mesoscale reinforced concrete. *Cement and Concrete Research*, 74, 95–107. https://doi.org/10.1016/j.cemconres.2015.04.008.

[25] Ožbolt, J., Balabanić, G., Periškić, G., & Kušter, M. (2010). Modelling the effect of damage on transport processes in concrete. *Construction and Building Materials, 24*(9), 1638–1648. https://doi.org/10.1016/j.conbuildmat.2010.02.028.

[26] Guzmán, S., Gálvez, J. C., & Sancho, J. M. (2012). Modelling of corrosion-induced cover cracking in reinforced concrete by an embedded cohesive crack finite element. *Engineering Fracture Mechanics*, 93, 92–107. https://doi.org/10.1016/j.engfracmech.2012.06.010.

[27] Guzmán, S., Gálvez, J. C., & Sancho, J. M. (2011). Cover cracking of reinforced concrete due to rebar corrosion induced by chloride penetration. *Cement and Concrete Research, 41*(8), 893–902. https://doi.org/10.1016/j.cemconres.2011.04.008.

[28] Jin, H., & Yu, S. (2022). Study on corrosion-induced cracks for the concrete with transverse cracks using an improved CDM-XFEM. *Construction and Building Materials*, 318, 126173 . https://doi.org/10.1016/j.conbuildmat.2021.126173.

[29] Zreid, I., & Kaliske, M. (2014). Regularization of microplane damage models using an implicit gradient enhancement. *International Journal of Solids and Structures, 51*(19–20). https://doi.org/10.1016/j.ijsolstr.2014.06.020.

[30] Zreid, I., & Kaliske, M. (2018). A gradient enhanced plasticity–damage microplane model for concrete. *Computational Mechanics, 62*(5). https://doi.org/10.1007/s00466-018-1561-1.

[31] Bažant, Z. P., & Gambarova, P. G. (1984). Crack Shear in Concrete: Crack Band Microplane Model. *Journal of Structural Engineering, 110*(9). https://doi.org/10.1061/(asce)0733-9445(1984)110:9(2015).

[32] Bažant, Z. P., & Prat, P. C. (1988). Microplane Model for Brittle Plastic Material: I. Theory. *Journal of Engineering Mechanics, 114*(10). https://doi.org/10.1061/(asce)0733-9399(1988)114:10(1672).

[33] ANSYS Inc. (2023). Material Reference, Canonsburg, USA.

[34] De Vree, J. H. P., Brekelmans, W. A. M., & van Gils, M. A. J. (1995). Comparison of nonlocal approaches in continuum damage mechanics. *Computers & Structures, 55*(4), 581–588. https://doi.org/10.1016/0045-7949(94)00501-S.

[35] Pamin, J. (2004). Gradient-enhanced continuum models: formulation, discretization and application. Cracow University of Technology.

[36] Wosatko, A. (2021). Comparison of evolving gradient damage formulations with different activity functions. *Archive of Applied Mechanics, 91*(2), 597–627. https://doi.org/10.1007/s00419-021-01889-2.

[37] The International Federation for Structural Concrete FIB. (2013). FIB Model Code for Concrete Structures 2010. In J. Walraven (Ed.), 2013 fédération internationale du béton/International Federation for Structural Concrete (fib). https://doi.org/10.1002/9783433604090.

[38] Jiang, H., & Zhao, J. (2015). Calibration of the continuous surface cap model for concrete. *Finite Elements in Analysis and Design*, 97, 1–19. https://doi.org/10.1016/j.finel.2014.12.002.